

Article

Fabrication of Six Manganese Containing Polyoxometalate Modified Graphite C₃N₄ Nanosheets Catalysts Used to Catalyze Water Decomposition

Yue Wu ^{1,*} , Xiaoxia Yu ¹, Zhijing Fu ², Jianye Pei ¹ and Lihua Bi ^{1,*}

¹ College of Chemistry, Jilin University, Changchun 130012, China; yuwx19@mails.jlu.edu.cn (X.Y.); peijy20@mails.jlu.edu.cn (J.P.)

² College of Water Resources and Environment, Hebei GEO University, Shijiazhuang 050031, China; fuzhijing@hgu.edu.cn

* Correspondence: wuyue17@mails.jlu.edu.cn (Y.W.); blh@jlu.edu.cn (L.B.)

Abstract: With the increase in gas population, the demand for clean and renewable energy is increasing. Hydrogen energy has a high combustion conversion energy while water is its combustion product. In recent years, a way to convert water into hydrogen and oxygen has been found by human beings inspired by plant photosynthesis. However, water decomposition consumes a significant amount of energy and is expensive. People expect to obtain a water decomposition catalyst with low cost and high efficiency. This work selected a six-manganese containing polyoxometalate with a similar structure characteristic to photosynthesizing PSII to fabricate with graphite C₃N₄ nanosheets for the construction of composite film (Mn₆SiW/g-C₃N₄NSs) electrode via layer by layer self-assembly technology, which was used for the photo-electrochemical decomposition of water under visible light conditions. The binary composite film electrode displayed good catalytic efficiency. The photoelectric density of the composite electrode is 46 μA/cm² (at 1.23 V vs. Ag/AgCl) and 239 μA/cm² (at 1.5 V vs. Ag/AgCl). Compared with the g-C₃N₄NSs electrode alone, the photoelectric density of the composite electrode increased by 1 time. The reason is attributed to the fact that Mn₆SiW has a similar structure characteristic to photosynthesizing PSII and high electron transferability. The construction of the composite film containing low-cost Mn₆SiW to modify g-C₃N₄NSs can effectively improve the photocatalytic decomposition of water, thus this study provides valuable reference information for the development of low-cost and high-performance photo-electrocatalytic materials.



Citation: Wu, Y.; Yu, X.; Fu, Z.; Pei, J.; Bi, L. Fabrication of Six Manganese Containing Polyoxometalate Modified Graphite C₃N₄ Nanosheets Catalysts Used to Catalyze Water Decomposition. *Catalysts* **2021**, *11*, 856. <https://doi.org/10.3390/catal11070856>

Academic Editor: Magdalena Janus

Received: 16 June 2021

Accepted: 14 July 2021

Published: 17 July 2021

Publisher's Note: MDPI stays neutral with regard to jurisdictional claims in published maps and institutional affiliations.



Copyright: © 2021 by the authors. Licensee MDPI, Basel, Switzerland. This article is an open access article distributed under the terms and conditions of the Creative Commons Attribution (CC BY) license (<https://creativecommons.org/licenses/by/4.0/>).

Keywords: graphite C₃N₄ nanosheets; water decomposition; oxygen evolution reaction; manganese containing polyoxometalate

1. Introduction

Currently, due to the influence of the greenhouse effect, global warming is a reality that causes serious damage to the earth's ecology. Glaciers in the polar regions are melting, and the average forest temperature in the tropical regions is increasing, which results in frequent fires and tens of thousands of animals losing their lives. Many studies have confirmed that the greenhouse effect is related to the carbon dioxide produced by the combustion of fossil fuels [1,2]. At the same time, fossil fuels are running out [3]. Mankind expects to eliminate its dependence on fossil fuels, and is seeking cleaner and renewable energy, such as electric energy [4], nuclear energy [5], solar energy [6], and biomass energy [7]. Solar energy refers to the light energy transmitted from the sun to the earth. As long as the sun and the earth exist, solar energy can be used all the time. Therefore, in the limited life of human beings, solar energy can be said to be inexhaustible. At present, reasonable utilization of solar energy includes solar cells [8], solar water heaters [9], photocatalytic organic pollutant degradation [10], photocatalytic water decomposition [11,12], and photosynthesis

in nature [13,14]. The main purpose of green plant photosynthesis in nature is to produce oxygen and hydrogen through photocatalysis. The oxygen produced is released to the outside of the body, and hydrogen combines with carbon dioxide to form organic molecules (e.g., glucose, etc.) [15]. The structure of photosystem II (PSII) has been determined by Ferreira et al. [16] (as shown in Figure 1).

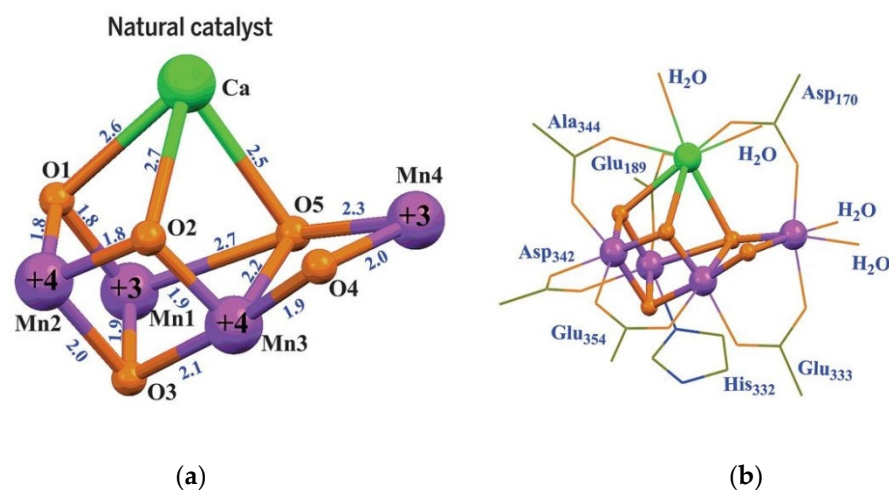


Figure 1. (a) Mn_4CaO_5 core of oxygen evolution catalyst (OEC) in nature; (b) Structure of the native OEC, involving ligating protein side-chains and water molecules. The bond lengths are given in Å; Mn, purple; Ca, green; O, orange; All H atoms and CH_3 groups have been omitted for clarity [16]. Reprinted with permission from ref. [16]. Copyright 2015 The American Association for the Advancement of Science.

Human beings, inspired by plant photosynthesis, have found a way to convert water into hydrogen and oxygen. Hydrogen is a kind of clean energy with high conversion energy, and its combustion product is water. At present, hydrogen has not been widely used commercially because of two reasons: first, the molecular weight of hydrogen is small, and the storage and transportation technology are not perfect; second, the generation of hydrogen is mainly from methane [11], but the byproduct carbon dioxide produced during the conversion process still plagues us. Water, as the main storage resource of hydrogen atoms, has a huge quantity, but it consumes a lot of energy, and it is expensive to convert it to hydrogen. Therefore, the development of a low-cost, high-efficiency method of hydrogen production from water decomposition is a research hotspot for current researchers. At present, the research on catalytic water decomposition has made progress in various fields, including organic catalysis [17], enzyme catalysis [18], inorganic semiconductor catalysis [19], coordination compound catalysis [20], etc. Each kind of catalyst has its own advantages and disadvantages. The synthesis cycle of organic catalyst is long, and the cost is high. The efficiency of a biocatalyst is high in a short time, but the stability of the biocatalyst is not very good because of the possibility of enzyme deactivation. Semiconductor catalysts are mainly used in the production of hydrogen by photocatalysis, but they display high recombination rate of photogenerated electron-holes and low photoelectric conversion efficiency. For example, graphite carbonitride ($g-C_3N_4$) is a two-dimensional semiconductor with an appropriate band gap (2.7 eV at 460 nm) [21]. It has a series of advantages, such as low cost, convenient synthesis and adjustable morphology, size and pore size distribution [22]. However, bulk $g-C_3N_4$ has a small specific surface area and a low carrier mobility, which can inhibit photoinduced reaction [23], whereas adjusting the surface morphology and oxygen doping can effectively improve the photocatalytic activity.

Coordination compound catalysts have various structures and excellent properties. As a kind of coordination compound, polyoxometalates (POMs) have been studied since 1912. POMs are the general term for a kind of metal oxygen cluster complex. They possess stable structures, good solubility in water, and an outstanding redox property. The charge

number of POMs can be adjusted from -3 to -14 . They can be synthesized with more than 70 elements, so they have more regulated properties. The catalytic activity of POMs for water decomposition has been reported [24]. These POMs usually have the structural characteristics of reversible continuous redox [25], exhibiting the ability of multi-electron storage and electron migration. These characteristics enable POMs to combine with semiconductor catalysts, so as to overcome the shortcomings of a high recombination rate of photogenerated electrons in the semiconductor, improve the photoelectric efficiency of the semiconductor, and improve the catalytic efficiency of the water decomposition. This method has been proved by Orlandi [24], Zhang [26], Lan [27], Yan [28] and Bi [29] et al. Among the POMs, there is a kind of POM with a similar structure to PSII [30,31], which usually contains transition metals, called a transition metal-substituted POM. Some manganese containing polyoxometalates (Mn-POMs) [32] not only have similar structures with OEC in nature, but also have the same manganese and oxygen elements. Therefore, it is expected that if the Mn-POMs are combined with the semiconductor $g\text{-C}_3\text{N}_4$ to form a co-catalyst, the catalytic efficiency of water decomposition under sunlight would be improved. Water decomposition includes oxygen and hydrogen evolution. As a critical step of water decomposition, oxygen evolution is more difficult to be completed due to the four-electron transfer. Accordingly, the development of the catalyst for the oxygen evolution reaction is required urgently. In this study, we selected a six-manganese containing polyoxometalate, $[\text{Mn}^{\text{III}}_2\text{Mn}^{\text{II}}_4(\mu_3\text{-O})_2(\text{H}_2\text{O})_4(\text{B-}\beta\text{-SiW}_8\text{O}_{31})(\text{B-}\beta\text{-SiW}_9\text{O}_{34})(\gamma\text{-SiW}_{10}\text{O}_{36})]^{18-}$ (Mn_6SiW), as shown in Figure 2, with a similar structure characteristic to photosynthesizing PSII, and fabricated with graphite C_3N_4 nanosheets to construct a composite film ($\text{Mn}_6\text{SiW}/g\text{-C}_3\text{N}_4\text{NSs}$) modified electrode by layer by layer self-assembly technology (LBL), via reasonable design and band gap matching. The obtained composite material $\text{Mn}_6\text{SiW}/g\text{-C}_3\text{N}_4\text{NSs}$ was used as photoelectrochemical (PEC) for water decomposition. Through the detailed characterization of the PEC catalyst and the catalysis experiments under visible light, it is proved that the PEC catalyst has good catalytic performance for water decomposition, can effectively promote the separation and transfer of photo generated electron hole pairs, and improve the rate of oxygen evolution. Hence, this study provides a low-cost and high-performance binary catalyst for a visible light driven photoelectrocatalytic system of water decomposition.

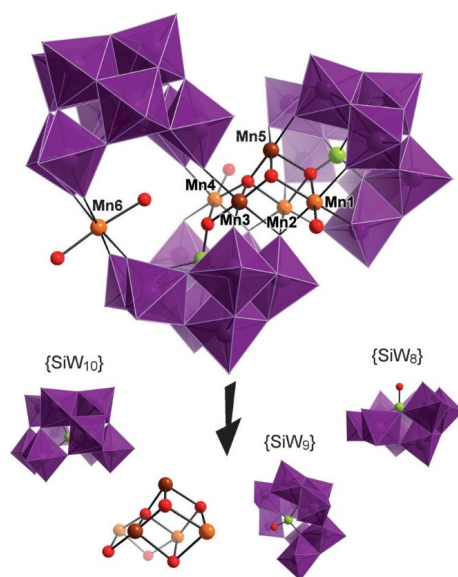


Figure 2. Structure of Mn_6SiW ; WO_6 polyhedra, purple; Mn, orange and brown; Si, green and O, red [33]. Reprinted with permission from ref. [33]. Copyright 2011 John Wiley and Sons.

2. Results and Discussion

2.1. Infrared Spectrum (IR) Test

In order to verify the compounds Mn_6SiW and $g\text{-C}_3\text{N}_4\text{NSs}$ were synthesized, their IR spectra were measured, as shown in Figure 3. It is clear in Figure 3a that the main characteristic vibration frequencies at 1628, 943, 854, 782, and 723 cm^{-1} , and two weak peaks at 455 and 437 cm^{-1} (the inset in Figure 3a) are observed, which are consistent with that of Mn_6SiW in the literature [33]. In addition, in Figure 3b, the IR spectrum of $g\text{-C}_3\text{N}_4\text{NSs}$ shows obvious peaks at 809, 1246–1634, 2990–3550 cm^{-1} , which are consistent with that of $g\text{-C}_3\text{N}_4\text{NSs}$ reported in the literature [34,35]. There are some small differences between the measured and reported values, which may be caused by the different instrument used. The observation above suggests that the compound Mn_6SiW and $g\text{-C}_3\text{N}_4\text{NSs}$ have been successfully prepared. See the Figure S1 in supporting information for a detailed description of the feature band.

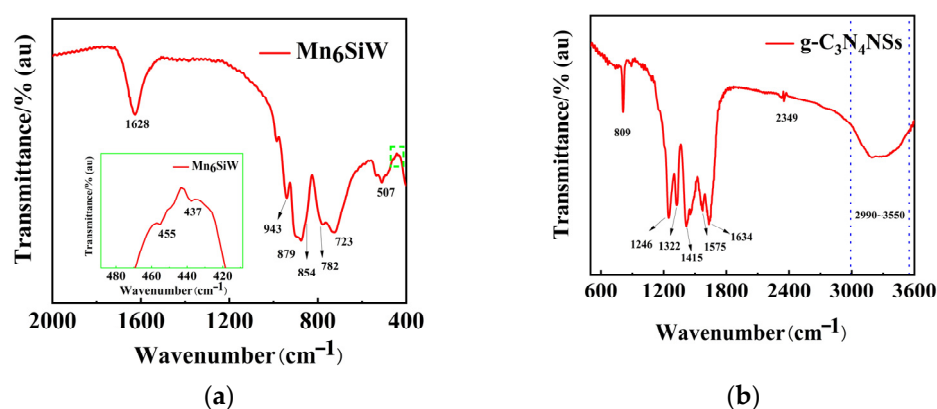


Figure 3. The IR spectra of Mn_6SiW (a) and (b) $g\text{-C}_3\text{N}_4\text{NSs}$.

2.2. Scanning Electron Micrograph (SEM)

Figure 4 shows the SEM image of $g\text{-C}_3\text{N}_4\text{NSs}$. In Figure 4a, the image presents a thin sheet structure of $g\text{-C}_3\text{N}_4\text{NSs}$. It can be seen from the color difference that the white part in the image means that the thickness of the nanosheet is very thin, so it is relatively transparent, whilst the darker part in the image is caused by the overlapping of multilayer nanosheets. Moreover, Figure 4b indicates the size of $g\text{-C}_3\text{N}_4\text{NSs}$ is about 500 nm after acidic treatment. Based on the images above, it can be found that the $g\text{-C}_3\text{N}_4\text{NSs}$ possess multilayer sheet structure, similar to graphene, so they are called graphite carbon nitride nanosheets.

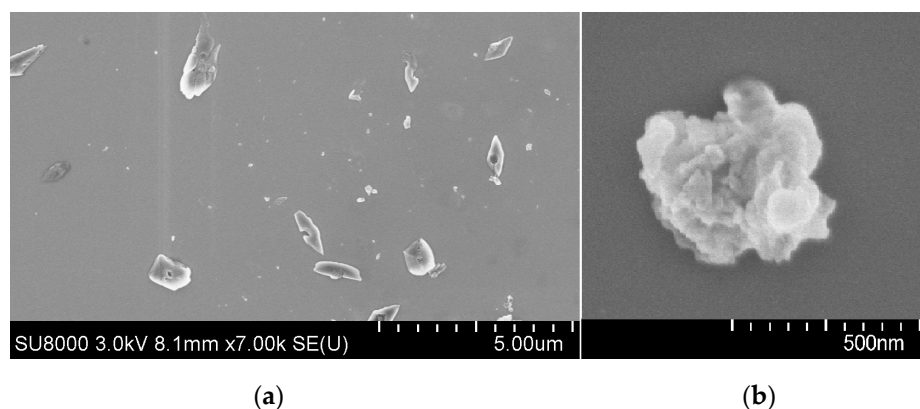


Figure 4. (a) and (b) SEM images of $g\text{-C}_3\text{N}_4\text{NSs}$.

2.3. UV-Vis Absorption Spectrum Test

From Figure 5a, it can be seen that the $g\text{-C}_3\text{N}_4\text{NSs}$ has a certain absorption peak in the visible region, while Mn_6SiW has an absorption peak at the 253 nm ultraviolet range. The

UV-vis spectrum of the mixture of $g\text{-C}_3\text{N}_4\text{NSs}$ and Mn_6SiW presents a wide absorption range in the ultraviolet and visible region, which is the reason why the $g\text{-C}_3\text{N}_4\text{NSs}$ and Mn_6SiW were chosen to construct the composite material. Additionally, according to the reports in the literature, the surface of components $g\text{-C}_3\text{N}_4\text{NSs}$ and Mn_6SiW have positive and negative charges, respectively. Therefore, the composite films based on $g\text{-C}_3\text{N}_4\text{NSs}$ and Mn_6SiW can be directly constructed by electrostatic interaction. The growth process of $[\text{g-C}_3\text{N}_4\text{NSs}/\text{Mn}_6\text{SiW}]_n$ was monitored by UV-Vis spectroscopy. As shown in Figure 5b, when comparing the absorption spectra of the components $g\text{-C}_3\text{N}_4\text{NSs}$ and Mn_6SiW in the composite film with that in the solution, it can be observed that the characteristic absorption peaks of $g\text{-C}_3\text{N}_4\text{NSs}$ and Mn_6SiW appear in the spectra of each layer, indicating that $g\text{-C}_3\text{N}_4\text{NSs}$ and Mn_6SiW have been assembled on the composite film. In addition, as shown in Figure 5c, the absorbance values at 253 nm for Mn_6SiW and 400 nm for $g\text{-C}_3\text{N}_4\text{NSs}$ were taken to plot the relationship with layer numbers of the composite film, and a high linear relationship was found between them, which proved that $g\text{-C}_3\text{N}_4\text{NSs}$ and Mn_6SiW grew uniformly on the composite film.

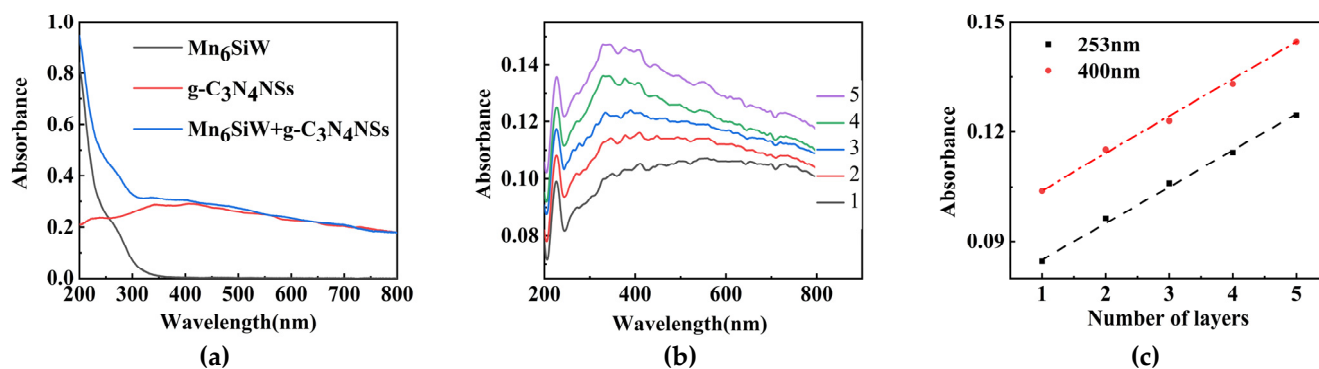


Figure 5. (a) UV-vis absorption spectra of $g\text{-C}_3\text{N}_4\text{NSs}$ (0.6 mM), Mn_6SiW (5 μM) and $g\text{-C}_3\text{N}_4\text{NSs}\text{-Mn}_6\text{SiW}$ (0.6 mM: 3 μM) mixture in the aqueous solutions; (b) UV-vis spectra for the $[\text{g-C}_3\text{N}_4\text{NSs}/\text{Mn}_6\text{SiW}]_n$ film on quartz slide; (c) relationship of the absorbance value and layer number at $\lambda = 253\text{ nm}$ and $\lambda = 400\text{ nm}$.

2.4. Electrochemical Characteristics

The electrochemical behaviors of Mn_6SiW in solution and composite film were studied, and the obtained cyclic voltammograms (CVs) were recorded. In Figure 6a, it is found that Mn_6SiW exhibits electrocatalytic activity towards water oxidation, although there is no light. This is because the Mn cluster in Mn_6SiW contains four divalent Mn and two trivalent Mn, which is similar with the component of OEC in nature, oxidizing OH^- in water to generate oxygen. Thus, the fabrication of the Mn_6SiW and $g\text{-C}_3\text{N}_4\text{NSs}$ composite film modified the electrode and would play a synergistic role in photoelectrocatalytic water oxidation. Figure 6b displays the CVs of Mn_6SiW in different pH solutions. It can be seen that the redox peak of Mn is reversible, and it shifts negatively with the increase in pH, indicating that Mn_6SiW can be stable in neutral condition and create high redox activity, thereby pH 7.0 was chosen as the condition of the follow-up test. Figure 6c shows that the oxidation peak current of $\text{Mn}^{\text{II/IV}}$ increases with the increase in the number of assembled layers, and a high linearly proportional relationship was observed in Figure 6d, indicating that the film assembly is homogeneous, which is consistent with that in UV-vis measurement.

2.5. PEC Oxygen Evolution Reaction (OER)

In order to study the PEC catalytic performance of $\text{Mn}_6\text{SiW}/g\text{-C}_3\text{N}_4\text{NSs}$ composite film electrode for water oxidation, the PEC tests were carried out. Figure 7a is the LSV curve of the $\text{Mn}_6\text{SiW}/g\text{-C}_3\text{N}_4\text{NSs}$ composite film electrode in NaAc/HAc (0.5 M, pH = 7.0) electrolyte. It can be observed that at the same potential, the current density of the composite film increases from 160.86 to 239.65 $\mu\text{A cm}^{-2}$ after irradiation, which is 1.49 times of that in the dark ($E = 1.5\text{ V vs. Ag}/\text{AgCl}$). When the potential is at 1.23 V (vs. Ag/AgCl),

the current density is increased from 33.16 to 46.22 $\mu\text{A cm}^{-2}$ after irradiation, which is 1.39 times of that in the dark (as shown in Table 1). It can be seen from Figure 7b that under simulated visible light, the initial catalytic potential of the composite film shifted negatively from 1.146 V to 1.10 V (Table 2). The reason is that under dark conditions, the $\text{Mn}_6\text{SiW/g-C}_3\text{N}_4\text{NSs}$ composite exhibits a certain catalytic effect on water oxidation. When irradiated by light, $\text{g-C}_3\text{N}_4\text{NSs}$ absorbs light energy, leading to separation of the electrons and holes, and then the electrons jump to the conduction band. In the composite film, due to the promotion of Mn_6SiW , the electron migration is accelerated, so that the catalytic current is increased, and the initial catalytic potential is shifted negatively, meaning that the overpotential of oxygen evolution is reduced, promoting water decomposition reaction.

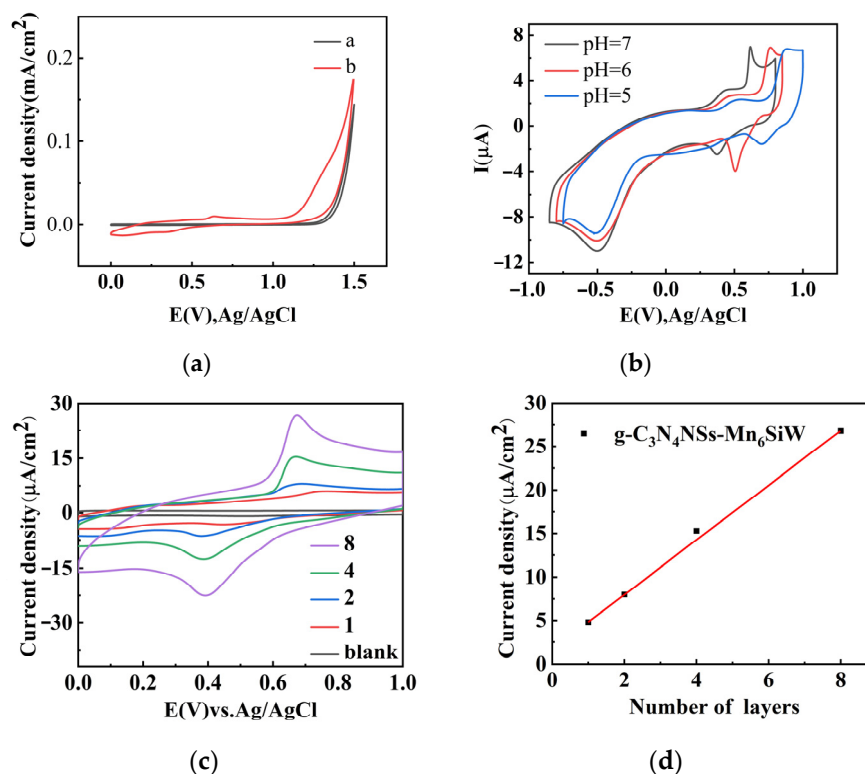


Figure 6. (a) Cyclic voltammogram (CV) curves of Mn_6SiW (0.6 mM, curve b) and blank solution (curve a) in NaAc/HAc buffer (0.5 M, pH = 7.0). (b) CV curves of Mn_6SiW in NaAc/HAc buffer (0.5 M) at different pH (5/6/7); (c) CV curves of the film ($\text{g-C}_3\text{N}_4\text{NSs/Mn}_6\text{SiW}$)_n in NaAc/HAc buffer (0.5 M, pH 7), $n = 1, 2, 4, 8$; at 50 mV/s; (d) the relationship between the oxidation peak current of $\text{Mn}^{\text{II/IV}}$ and the number of assembled layers.

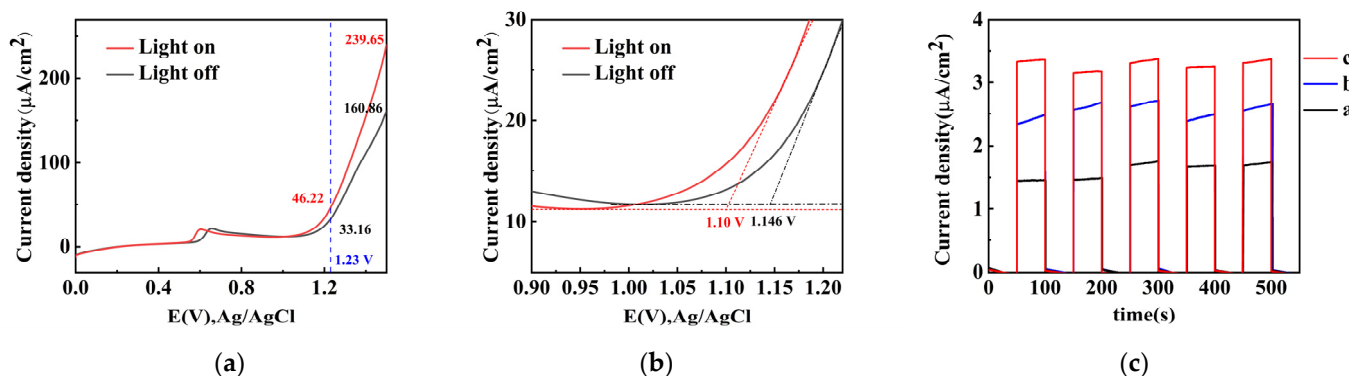


Figure 7. (a) LSV of ($\text{g-C}_3\text{N}_4\text{NSs/Mn}_6\text{SiW}$)₂ film electrode in light on (red) and light off (black); (b) The locally enlarged graph of (a); (c) amperometric i-t Curve of the ($\text{g-C}_3\text{N}_4\text{/PSS}$)₂ film (a), (PDDA/ Mn_6SiW)₂ film (b), and ($\text{g-C}_3\text{N}_4\text{NSs/Mn}_6\text{SiW}$)₂ film (c) under incandescent lamp irradiation (450–650 nm).

Table 1. The current density of PDDA/PSS/(g-C₃N₄NSs/Mn₆SiW)₂-ITO electrode.

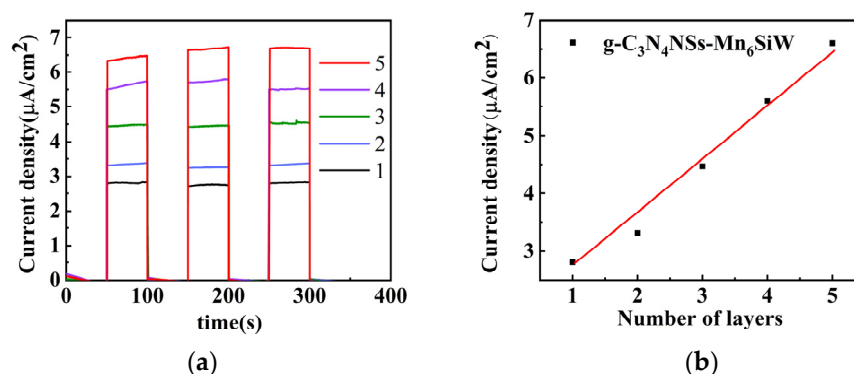
E (V vs. Ag/AgCl)	Current Density ($\mu\text{A cm}^{-2}$)	
	Light Off	Light on
1.23	33.16	46.22
1.50	160.86	239.65

Table 2. The catalytic potential of PDDA/PSS/(g-C₃N₄NSs/Mn₆SiW)₂-ITO electrode.

PDDA/PSS/(g-C ₃ N ₄ NSs/Mn ₆ SiW) ₂ -ITO	E (V) _{on}
Light on	1.100
Light off	1.146

In order to compare the PEC performance of three electrodes, (g-C₃N₄NSs/PSS)₂ film (a), (PDDA/Mn₆SiW)₂ film (b), and (g-C₃N₄NSs/Mn₆SiW)₂ film (c) for water oxidation, their *i*-*t* curves were measured at the applied voltage of 1.5 V (vs. Ag/AgCl). As shown in Figure 7c, the photocurrents of all electrodes are stable and repeatable. It can be seen that the photocurrent response of g-C₃N₄NSs is the lowest in light on and dark, which is mainly due to the rapid recombination of photogenerated electrons and holes in g-C₃N₄NSs. The photocurrent of Mn₆SiW electrode is higher than that of g-C₃N₄NSs. The photocurrent of Mn₆SiW/g-C₃N₄NSs electrode at 1.23 V is twice as high as that of g-C₃N₄NSs. The main reason is that Mn₆SiW cannot only effectively promote the electron transfer at the interface, but can also improve the photocurrent response, owing to the characteristics of the semiconductor. It is worth noting that the Mn₆SiW/g-C₃N₄NSs electrode has the strongest photoelectric response, which further indicates that Mn₆SiW promotes the photoelectric conversion efficiency of g-C₃N₄NSs. These results show that the Mn₆SiW/g-C₃N₄NSs composite electrode has good performance for photoelectrocatalytic oxidation of water.

In order to further verify the effect of the layer number of the composite film electrode on the PEC water oxidation, we assembled a multilayer film electrode with different layer numbers and tested their photocurrent response. It can be seen from Figure 8 that with the increase in the layer number of the composite film electrode, the photocurrent density also increases, showing a linear relationship between the photocurrent density and layer number, suggesting that PEC activity of the Mn₆SiW/g-C₃N₄NSs film electrode for water oxidation is adjustable.

**Figure 8.** (a) Amperometric *i*-*t* curves of the PDDA/PSS/(g-C₃N₄NSs/Mn₆SiW)_n film (*n* = 1–5) under incandescent lamp irradiation (450–650 nm); (b) the relationship between average of photocurrent and number of film electrode assembly layers.

In Table 3, we compared with other reported polyoxometalate modified C₃N₄ catalysts for catalytic water decomposition. It can be seen that, although using energy-saving lamps with low energy, our designed composite film catalyst still displays high PEC activity for water oxidation.

Table 3. Reported polyoxometalate modified C₃N₄ catalysts used to catalyze water decomposition.

PEC Catalysts	Light Source	Current Density	Growth Multiple (vs. C ₃ N ₄)	Ref.
SiW ₁₂ /C ₃ N ₄	Xe lamp (300 W)	$2.1 \times 10^{-4} \mu\text{A}/\text{cm}^2$ (E = 1.23 vs. RHE)	1.4	[36]
P ₅ W ₃₀ /g-C ₃ N ₄	Xe lamp (400 W)	44 $\mu\text{A}/\text{cm}^2$ (E = 1.23 V vs. RHE)	2.4	[37]
Mn ₆ SiW/g-C ₃ N ₄ NSs	Energy-saving lamps (150 W)	46 $\mu\text{A}/\text{cm}^2$ (E = 1.23 V vs. Ag/AgCl) 239 $\mu\text{A}/\text{cm}^2$ (E = 1.5 V vs. Ag/AgCl)	2	Our work

3. Materials and Methods

3.1. Materials and Apparatus

3.1.1. Materials

Poly (diallyldimethylammonium chloride) (PDDA) (Mw = 10,000–20,000) and poly (4-styrene sulfonic acid) sodium salt (PSS) were obtained from Sigma Aldrich (Merck KGaA, Darmstadt, Germany). Sodium tungstate (Na₂WO₄·2H₂O), sodium metasilicate (Na₂SiO₃·5H₂O), sodium hydroxide (NaOH), manganese chloride (MnCl₂), potassium carbonate (K₂CO₃), hydrochloric acid (HCl), potassium chloride (KCl), and ethanol were analytical grade and used as received. Water was purified by Millipore Milli-Q (Merck Millipore, Darmstadt, Germany).

3.1.2. Apparatus

PHS–25B digital acidimeter (Yuechen, Shanghai, China), determined pH value. The infrared spectra (IR) were measured on a spectrometer (Bruker Vertex 80V, Bruker, Karlsruhe, Germany). Absorption measurements (UV-vis) were completed with UV-2700 UV-Visible spectrophotometer (Shimadzu, Kyoto, Japan). The cyclic voltammetry curve (CV), the linear sweep voltammetry curve (LSV), and the current–time relationship (I–T) were recorded using CHI660e electrochemical workstation (Shanghai Chenhua Instrument Co., Ltd., Shanghai, China).

3.2. Preparation of Electrode Modified Materials

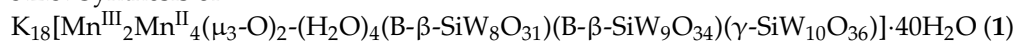
3.2.1. Synthesis of K₈[β₂-SiW₁₁O₃₉]·14H₂O (**1a**)

The precursors K₈[β₂-SiW₁₁O₃₉]·14H₂O and K₈[γ-SiW₁₀O₃₉]·12H₂O (**1b**) were synthesized according to the published procedure [38]. An amount of 18.2 g Na₂WO₄·2H₂O was dissolved in 30 mL water, and 16.5 mL 4 M HCl was slowly added to the solution and stirred for 10 min. An amount of 1.1 g of Na₂SiO₃·5H₂O was dissolved in 10 mL of water, then poured into the above solution and adjusted from pH 5 to 6 with 4 M HCl solution. An amount of 9 g KCl was added to the solution by stirring. After 15 min, the precipitate was filtered, washed with 2M KCl and dried.

3.2.2. Synthesis of K₈[γ-SiW₁₀O₃₉]·12H₂O (**1b**)

At room temperature, 3 g **1a** was dissolved in 30 mL water to remove the insoluble matter quickly. Using 2 M K₂CO₃ aqueous solution, the pH value of the solution was quickly adjusted to 9.1, and maintained for 16 min. An amount of 8 g KCl was added to the solution for precipitation while maintaining the pH value. After 10 min, the solution was filtered, washed with 1 M KCl solution, and air dried.

3.2.3. Synthesis of



The mixed-valence Mn6-containing polyoxometalates were synthesized according to the literature reported by Mitchell et al. [33]. An amount of 1.45 g **1b** was dissolved in 25 mL water and heat to 40 °C. When the temperature reached 38 °C, 0.13 g MnCl₂ was added

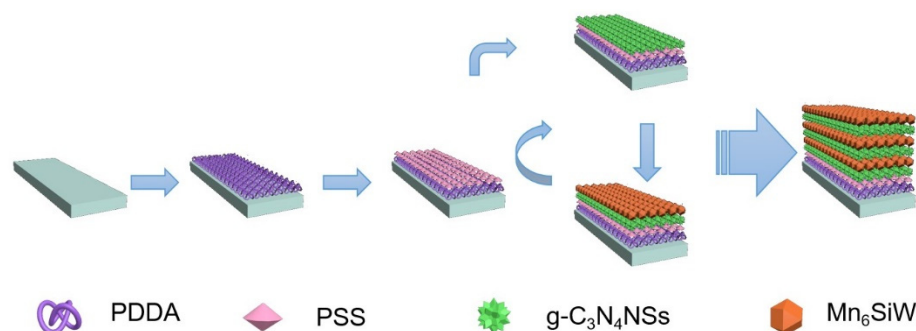
by stirring. The pH value of the solution was adjusted to 8.40 with 2 M K_2CO_3 solution. The pH value of the solution was adjusted from 8.40 to 8.50 with 0.2 M K_2CO_3 solution and maintained for 40 min. The solution turned dark brown. The stirring was then continued at 40 °C for 4 h, before the solution was cooled to room temperature. The brown precipitates were removed by centrifugation (5 min at 4400 rpm) to obtain a dark brown solution, which was poured into a wide necked conical flask and crystallized overnight at 18 °C.

3.2.4. Synthesis of Protonated Graphitic Carbon Nitride Nanosheets (g- C_3N_4 NSs)

The g- C_3N_4 NSs was synthesized according to the literature of Fu et al. [34]. An amount of 5.0 g melamine was put in a crucible, heated in a muffle furnace to 500 °C for 2 h, and then raised to 550 °C for 4 h. The yellow powder g- C_3N_4 was obtained. Then, g- C_3N_4 was dispersed into 30 mL of 5M HNO_3 solution, stirred for 3 h, and then refluxed at 125 °C for 24 h. After centrifugation, the solution was washed repeatedly with water until pH = 7, and then dried in vacuum for 12 h (60 °C).

3.2.5. LBL Assembled Composite Film Modified Electrode

Before assembly, the substrate (ITO electrode) needed to be cleaned according to the literature [39]. The ITO was immersed in 1 M NaOH: CH_3CH_2OH (V:V = 1:1) mixed solution, ultrasonically for 20 min, then cleaned with water, and then dried with nitrogen for standby. Then, the composite film was assembled on the clean substrate by the LbL assembly method (as shown in Scheme 1). First, the substrate was immersed in the positively charged PDDA (8%) solution and left to stand for 20 min. Second, the substrate was immersed in the negatively charged PSS solution for 20 min. Third, the substrate was immersed in the g- C_3N_4 NSs (1.0 mg mL^{-1}) aqueous solution for 20 min. Fourth, the substrate was immersed in 0.5 mM Mn_6SiW solution with negative charge for 20 min. After each assembly, the substrate was washed with water 3–5 times to remove the physical adsorption substances, and then dried with nitrogen flow. After the above steps, the monolayer [PDDA/PSS/g- C_3N_4 NSs/ Mn_6SiW] composite films were prepared. Different layers of [PDDA/PSS/g- C_3N_4 NSs/ Mn_6SiW] $_n$ -ITO ($n = 1-8$) composite film modified electrodes were prepared by repeating steps 3 and 4.



Scheme 1. The assembly process diagram of Mn_6SiW and g- C_3N_4 NSs composite films by LBL.

3.3. UV-Vis Absorption Spectra

The fabrication process of the samples is the same as that of the LBL assembling the multilayer film modified electrode in Section 3.2.5. The only difference is that ITO is replaced by a quartz slide. Firstly, the quartz glass was cleaned according to the literature method (different from ITO) [40], and then assembled according to the film assembly steps, monitoring the assembly process of composite films by UV-vis absorption spectrum.

3.4. Photo-Electrochemical Test

A series of experiments were performed to study the PEC catalytic activity for water oxidation, ITO/PDDA/PSS/[g- C_3N_4 NSs/ Mn_6SiW] $_n$ was used as the working electrode, using Ag/AgCl as a reference electrode, and a platinum wire as a counter electrode. The buffer solution was obtained from 0.5 M pH 7 CH_3COONa (NaAc) solutions adjusted by

CH₃COOH (HAc). Before the electrochemical experiments, the oxygen in the electrolyte was removed by purging high-purity nitrogen. All the electrochemical measurements were performed on an electrochemical workstation (CHI 611E, CH Instruments Co., Bee Cave, TX, USA) at room temperature. An ordinary fluorescent energy-saving lamp was used as visible light source (wavelength range ≥ 380 , 150 W). A quartz cell was used as a reaction tank, about 10 cm from the light source.

4. Conclusions

In summary, Mn₆SiW/g-C₃N₄NSs composite film electrode was prepared by using layer by layer self-assembly technology and low-cost inorganic materials of non-precious metals. It was used for PEC catalytic water oxidation to generate oxygen. The results proved that the binary composite film electrode displayed high catalytic efficiency. The photoelectric density of the binary composite electrode reached 239 $\mu\text{A}/\text{cm}^2$ (E = 1.5V vs. Ag/AgCl). Compared to the simple g-C₃N₄NSs electrode, the photoelectric density of the binary composite electrode is two times stronger. Therefore, using low-cost Mn₆SiW to modify g-C₃N₄NSs can effectively improve the photoelectrocatalytic performance of C₃N₄ for water decomposition. Therefore, this study provides valuable reference information for the development of low-cost and high-performance photoelectrocatalytic materials.

Supplementary Materials: The following are available online at <https://www.mdpi.com/article/10.3390/catal11070856/s1>, Figure S1: The IR spectra of g-C₃N₄NSs.

Author Contributions: Conceptualization, Y.W. and L.B.; validation, Y.W., X.Y. and J.P.; formal analysis, Y.W.; investigation, Y.W., X.Y. and J.P.; resources, Y.W. and Z.F.; data curation, Y.W.; writing—original draft preparation, Y.W.; writing—review and editing, Y.W. and L.B.; visualization, Y.W.; supervision, L.B.; All authors have read and agreed to the published version of the manuscript.

Funding: This research received no external funding.

Data Availability Statement: The data presented in this study are available on request from the corresponding author. The data are not publicly available due to the need of follow-up research.

Acknowledgments: Thank the professor and co-author for their help in writing this article. Thank the reviewers for their comments and valuable opinions, and the editors for their help in publishing this article.

Conflicts of Interest: The authors declare no conflict of interest.

References

1. Archer, D.; Eby, M.; Brovkin, V.; Ridgwell, A.; Cao, L.; Mikolajewicz, U.; Caldeira, K.; Matsumoto, K.; Munhoven, G.; Montenegro, A.; et al. Atmospheric Lifetime of Fossil Fuel Carbon Dioxide. *Annu. Rev. Earth Planet. Sci.* **2009**, *37*, 117–134. [CrossRef]
2. Lincoln, S.F. Fossil fuels in the 21st century. *Ambio* **2005**, *34*, 621–627. [CrossRef] [PubMed]
3. Shafiee, S.; Topal, E. When will fossil fuel reserves be diminished? *Energy Policy* **2009**, *37*, 181–189. [CrossRef]
4. Wang, J.; Zhao, X.; Guo, X.; Li, B. Analyzing the research subjects and hot topics of power system reliability through the Web of Science from 1991 to 2015. *Renew. Sustain. Energy Rev.* **2018**, *82*, 700–713. [CrossRef]
5. Zinkle, S.J.; Was, G.S. Materials challenges in nuclear energy. *Acta Mater.* **2013**, *61*, 735–758. [CrossRef]
6. Liu, L.-Q.; Wang, Z.-X.; Zhang, H.-Q.; Xue, Y.-C. Solar energy development in China—A review. *Renew. Sustain. Energy Rev.* **2010**, *14*, 301–311. [CrossRef]
7. Parikka, M. Global biomass fuel resources. *Biomass Bioenergy* **2004**, *27*, 613–620. [CrossRef]
8. Chen, L.; Chen, W.-L.; Wang, X.-L.; Li, Y.-G.; Su, Z.-M.; Wang, E.-B. Polyoxometalates in dye-sensitized solar cells. *Chem. Soc. Rev.* **2019**, *48*, 260–284. [CrossRef]
9. Kalogirou, S. Thermal performance, economic and environmental life cycle analysis of thermosiphon solar water heaters. *Sol. Energy* **2009**, *83*, 39–48. [CrossRef]
10. Hill, C.L.; Bouchard, D.A. Catalytic photochemical dehydrogenation of organic substrates by polyoxometalates. *J. Am. Chem. Soc.* **1985**, *107*, 5148–5157. [CrossRef]
11. Bak, T.; Nowotny, J.; Rekas, M.; Sorrell, C. Photo-electrochemical hydrogen generation from water using solar energy. Materials-related aspects. *Int. J. Hydrogen Energy* **2002**, *27*, 991–1022. [CrossRef]
12. Kudo, A.; Miseki, Y. Heterogeneous photocatalyst materials for water splitting. *Chem. Soc. Rev.* **2009**, *38*, 253–278. [CrossRef] [PubMed]
13. Calvin, M. Solar Energy by Photosynthesis. *Science* **1974**, *184*, 375–381. [CrossRef] [PubMed]

14. Kruse, O.; Rupprecht, J.; Mussgnug, J.H.; Dismukes, G.C.; Hankamer, B. Photosynthesis: A blueprint for solar energy capture and biohydrogen production technologies. *Photochem. Photobiol. Sci.* **2005**, *4*, 957–970. [[CrossRef](#)] [[PubMed](#)]
15. Barber, J. Biological solar energy. *Philos. Trans. R. Soc. A Math. Phys. Eng. Sci.* **2007**, *365*, 1007–1023. [[CrossRef](#)]
16. Zhang, C.; Chen, C.; Dong, H.; Shen, J.-R.; Dau, H.; Zhao, J. A synthetic Mn₄Ca-cluster mimicking the oxygen-evolving center of photosynthesis. *Science* **2015**, *348*, 690–693. [[CrossRef](#)]
17. Steier, L.; Holliday, S. A bright outlook on organic photoelectrochemical cells for water splitting. *J. Mater. Chem. A* **2018**, *6*, 21809–21826. [[CrossRef](#)]
18. Mersch, D.; Lee, C.-Y.; Zhang, J.; Brinkert, K.; Fontecilla-Camps, J.C.; Rutherford, A.; Reisner, E. Wiring of Photosystem II to Hydrogenase for Photoelectrochemical Water Splitting. *J. Am. Chem. Soc.* **2015**, *137*, 8541–8549. [[CrossRef](#)]
19. Arunachalam, P.; Nagai, K.; Amer, M.S.; Ghanem, M.A.; Ramalingam, R.J.; Al-Mayouf, A.M. Recent Developments in the Use of Heterogeneous Semiconductor Photocatalyst Based Materials for a Visible-Light-Induced Water-Splitting System—A Brief Review. *J. Catal.* **2021**, *11*, 1–27.
20. Nesterov, D.S.; Nesterova, O.V. Polynuclear Cobalt Complexes as Catalysts for Light-Driven Water Oxidation: A Review of Recent Advances. *J. Catal.* **2018**, *8*, 602. [[CrossRef](#)]
21. Qiu, Y.; Xing, Z.; Guo, M.; Zhao, T.; Wang, Y.; Chen, P.; Li, Z.; Pan, K.; Zhou, W. Cadmium sulfide quantum dots/dodecahedral polyoxometalates/oxygen-doped mesoporous graphite carbon nitride with Z-scheme and Type-II as tandem heterojunctions for boosting visible-light-driven photocatalytic performance. *J. Colloid Interface Sci.* **2021**, *582*, 752–763. [[CrossRef](#)] [[PubMed](#)]
22. Ghattavi, S.; Nezamzadeh-Ejhi, A. A visible light driven AgBr/g-C₃N₄ photocatalyst composite in methyl orange photodegradation: Focus on photoluminescence, mole ratio, synthesis method of g-C₃N₄ and scavengers. *Compos. Part B Eng.* **2020**, *183*, 107712. [[CrossRef](#)]
23. Liu, J.; Xu, H.; Xu, Y.; Song, Y.; Lian, J.; Zhao, Y.; Wang, L.; Huang, L.; Ji, H.; Li, H. Graphene quantum dots modified meso-porous graphite carbon nitride with significant enhancement of photocatalytic activity. *Appl. Catal. B Environ.* **2017**, *207*, 429–437. [[CrossRef](#)]
24. Orlandi, M.; Argazzi, R.; Sartorel, A.; Carraro, M.; Scorrano, G.; Bonchio, M.; Scandola, F. Ruthenium polyoxometalate water splitting catalyst: Very fast hole scavenging from photogenerated oxidants. *Chem. Commun.* **2010**, *46*, 3152–3154. [[CrossRef](#)] [[PubMed](#)]
25. Geletii, Y.V.; Yin, Q.; Hou, Y.; Huang, Z.; Ma, H.; Song, J.; Besson, C.; Luo, Z.; Cao, R.; O'Halloran, K.P.; et al. Polyoxometalates in the Design of Effective and Tunable Water Oxidation Catalysts. *Isr. J. Chem.* **2011**, *51*, 238–246. [[CrossRef](#)]
26. Zhang, Z.; Lin, Q.; Kurunthu, D.; Wu, T.; Zuo, F.; Zheng, S.; Bardeen, C.J.; Bu, X.; Feng, P. Synthesis and Photocatalytic Properties of a New Heteropolyoxoniobate Compound: K₁₀[Nb₂O₂(H₂O)₂][SiNb₁₂O₄₀]-12H₂O. *J. Am. Chem. Soc.* **2011**, *133*, 6934–6937. [[CrossRef](#)] [[PubMed](#)]
27. Lan, Q.; Zhang, Z.-M.; Qin, C.; Wang, X.-L.; Li, Y.-G.; Tan, H.-Q.; Wang, E.-B. Highly Dispersed Polyoxometalate-Doped Porous Co₃O₄ Water Oxidation Photocatalysts Derived from POM@MOF Crystalline Materials. *Chem. A Eur. J.* **2016**, *22*, 15513–15520. [[CrossRef](#)]
28. Wu, Y.; Bi, L. Research Progress on Catalytic Water Splitting Based on Polyoxometalate/Semiconductor Composites. *J. Catal.* **2021**, *11*, 524. [[CrossRef](#)]
29. Zhou, Q.; Du, Y.; Qu, Z.; Bi, L. Facile multilayer assemble of a mixed-valence Mn⁴⁺-containing silicotungstate and its electrochemical study with Co₃O₄ as co-catalyst for photoelectrocatalytic water oxidation. *J. Electroanal. Chem.* **2021**, *894*, 1–11. [[CrossRef](#)]
30. Han, X.-B.; Zhang, Z.-M.; Zhang, T.; Li, Y.-G.; Lin, W.; You, W.; Su, Z.-M.; Wang, E.-B. Polyoxometalate-Based Cobalt-Phosphate Molecular Catalysts for Visible Light-Driven Water Oxidation. *J. Am. Chem. Soc.* **2014**, *136*, 5359–5366. [[CrossRef](#)] [[PubMed](#)]
31. Wei, J.; Feng, Y.; Zhou, P.; Liu, Y.; Xu, J.; Xiang, R.; Ding, Y.; Zhao, C.; Fan, L.; Hu, C. A Bioinspired Molecular Polyoxometalate Catalyst with Two Cobalt (II) Oxide Cores for Photocatalytic Water Oxidation. *ChemSusChem* **2015**, *8*, 2630–2634. [[CrossRef](#)]
32. Al-Oweini, R.; Sartorel, A.; Bassil, B.S.; Natali, M.; Berardi, S.; Scandola, F.; Kortz, U.; Bonchio, M. Photocatalytic Water Oxidation by a Mixed-Valent Mn^{III}₃Mn^{IV}O₃ Manganese Oxo Core that Mimics the Natural Oxygen-Evolving Center. *Angew. Chem. Int. Ed.* **2014**, *53*, 11182–11185. [[CrossRef](#)]
33. Mitchell, S.G.; Molina, P.I.; Khanra, S.; Miras, H.N.; Cronin, L. A Mixed-Valence Manganese Cubane Trapped by Inequiv-alent Trilacunary Polyoxometalate Ligands. *Angew. Chem.* **2011**, *50*, 9154–9157. [[CrossRef](#)]
34. Fu, Z.; Ma, Z.; Yu, T.; Bi, L.; Tian, Y. A first blue fluorescence composite film based on graphitic carbon nitride nanosheets/polyoxometalate for application in reversible electroluminescence switching. *J. Mater. Chem. C* **2019**, *7*, 3253–3262. [[CrossRef](#)]
35. Xu, J.; Zhang, L.; Shi, R.; Zhu, Y. Chemical exfoliation of graphitic carbon nitride for efficient heterogeneous photocatalysis. *J. Mater. Chem. A* **2013**, *1*, 14766–14772. [[CrossRef](#)]
36. Yan, G.; Feng, X.; Xiao, L.; Xi, W.; Tan, H.; Shi, H.; Wang, Y.; Li, Y. Tuning of the photocatalytic performance of g-C₃N₄ by polyoxometalates under visible light. *Dalton Trans.* **2017**, *46*, 16019–16024. [[CrossRef](#)] [[PubMed](#)]
37. Yousefi, M.; Eshghi, H.; Karimi-Nazarabad, M.; Farhadipour, A. P5W30/g-C₃N₄ heterojunction thin film with improved photoelectrochemical performance for solar water splitting. *New J. Chem.* **2020**, *44*, 20470–20478. [[CrossRef](#)]
38. Ginsberg, A.P. *Inorganic Syntheses*; John Wiley & Sons: Hoboken, NJ, USA, 1990; Volume 27.

-
39. Shen, Y.; Liu, J.Y.; Jiang, J.G.; Liu, B.F.; Dong, S.J. Fabrication of a metalloporphyrin—Polyoxometalate hybrid film by a layer-by-layer method and its catalysis for hydrogen evolution and dioxygen reduction. *J. Phys. Chem. B* **2003**, *107*, 9744–9748. [[CrossRef](#)]
 40. Huang, M.; Bi, L.; Shen, Y.; Liu, A.B.; Dong, S. Nanocomposite Multilayer Film of Preyssler-Type Polyoxometalates with Fine Tunable Electrocatalytic Activities. *J. Phys. Chem. B* **2004**, *108*, 9780–9786. [[CrossRef](#)]